

1 **Reveal a hidden highly toxic substance in biochar to**
 2 **support its effective elimination strategy**

3 Jiewen Luo¹, Litao Lin^{1,2}, Cun Liu³, Chao Jia¹, Tianyue Chen⁴, Yang Yang⁵, Minghao
 4 Shen¹, Hua Shang¹, Shaojie Zhou¹, Meiyong Huang³, Yujun Wang³, Dongmei Zhou⁶,
 5 Jiajun Fan⁷, James H. Clark^{1,7}, Shicheng Zhang^{1, 8, 9}, Xiangdong Zhu^{1, 8, 9*}

6
 7 ¹ *Shanghai Key Laboratory of Atmospheric Particle Pollution and Prevention (LAP3),*
 8 *Department of Environmental Science and Engineering, Fudan University, Shanghai*
 9 *200438, China*

10 ² *School of Energy and Power Engineering, Jiangsu University of Science and Technology,*
 11 *Zhenjiang, Jiangsu 212003, China*

12 ³ *Key Laboratory of Soil Environment and Pollution Remediation, Institute of Soil Science,*
 13 *Chinese Academy of Sciences, Nanjing 210008, China*

14 ⁴ *School of Mathematical Science, Fudan University, Shanghai 200438, China*

15 ⁵ *Bioenergy Research Group, European Bioenergy Research Institute, Aston University,*
 16 *Birmingham B4 7ET, UK*

17 ⁶ *School of the Environment, Nanjing University, Xianlin Ave. 163, Nanjing 210023, China*

18 ⁷ *Green Chemistry Centre of Excellence, Department of Chemistry, University of York,*
 19 *York, YO10 5DD, UK*

20 ⁸ *Shanghai Institute of Pollution Control and Ecological Security, Shanghai 200092, China*

21 ⁹ *Shanghai Technical Service Platform for Pollution Control and Resource Utilization of*

22 *Organic Wastes, Shanghai 200438, China*

23 * Corresponding Author. Phone: +86 3124 2297; e-mail: zxdjewett@fudan.edu.cn

24 (Xiangdong Zhu).

25

26 **ABSTRACT**

27 With the aim to develop optimized biochar with minimal contaminants, it is important
28 significance to broaden the understanding of biochar. Here, we disclose for the first time,
29 a highly toxic substance (metal cyanide, MCN, such as KCN or NaCN) in biochar. The
30 cyanide ion (CN⁻) content in biochar can be up to 85870 mg/kg, which is determined by
31 the inherent metal content and type in the biomass with K and Na increasing and Ca, Mg
32 and Fe decreasing its formation. Density functional theory (DFT) analysis shows that
33 unstable alkali oxygen-containing metal salts such as K₂CO₃ can induce an N
34 rearrangement reaction to produce for example, KOCN. The strong reducing character of
35 the carbon matrix further converts KOCN to KCN, thus resulting biochar with high risk.
36 However, the stable Mg, Ca and Fe salts in biomass cannot induce an N rearrangement
37 reaction due to their high binding energies. We therefore propose that high valent metal
38 chloride salts such as FeCl₃ and MgCl₂ could be used to inhibit the production of cyanide
39 *via* metal interactive reaction. These findings open a new point of view on the potential
40 risk of biochar and provide a mitigation solution for biochar's sustainable application.

41 *Keywords: Biochar, Toxic substance, Metal cyanide, Theoretical calculation*

42

43 **1. Introduction**

44 Biochar is globally recognized as a positive contributor to reducing the challenges of
45 soil degradation (through increasing soil nutrient retention) and combating climate change
46 (by carbon sequestration and reducing soil-borne greenhouse gas emissions) (Yue et al.,
47 2019; Chen et al., 2020; Quan et al., 2020). Clearly the composition of the biochar is of
48 vital importance including minimizing toxins (Lu et al., 2018). Previous research has
49 pointed to the potential presence of some problematic substances including polycyclic
50 aromatic hydrocarbons (PAHs) (Keiluweit et al., 2012; Zhao et al., 2020), heavy metals
51 and other elements (such as Cd, Pb, Cu, Zn, and As) (Freddo et al., 2012; Stefaniuk et
52 al., 2016), water dissolved organic matters (WDOMs) (Smith et al., 2016; Ghidotti et al.,
53 2017) and persistent free radicals (Liao et al., 2014; Lieke et al., 2018). Consequently, a
54 series of studies have been performed on the effects of such hazardous chemicals since
55 they can induce biotoxicity inhibiting germination, causing tissue damage and cytotoxicity
56 (Oleszczuk et al., 2013; Sigmund et al., 2017; Hao et al., 2018; Zhang et al., 2019).

57 Very recently, studies have shown that organic nitrogen and metals can combine and
58 react to form some new N-containing metal substances such as (metal cyanides, MCN)
59 (Tsubouchi et al., 2016; Sevilla et al., 2018; Luo et al., 2019). Metal elements and organic
60 N are commonly found in biomass (Sun et al., 2013; Qiu et al., 2015). Therefore, it can
61 be inferred that biochar can carry this toxic substance (i.e., MCN), especially a biochar
62 produced from a biomass with high content of metals and organic N (i.e., foodwaste,

63 sludge, fungi residues, alga). Its presence or at least the possibility of its presence will
64 have a major negative impact on the perceived value of biochar. Recently, biochar has
65 been one of the reasons shown to have high biotoxicity on plant growth and while this
66 could be due to several possible toxic contaminants (Hameed et al., 2019). Undoubtedly,
67 MCN contamination will reinforce such observations.

68 Clearly an effective MCN controlling strategy is vital to support the sustainable
69 application of biochar and the method must be applicable to a wide range of potential
70 biochar feedstocks, such as agricultural straw, biogas residue, drug residues, livestock
71 manure, and food waste (Zhang et al., 2014a; Opatokun et al., 2015; Zhang et al., 2015;
72 Wang et al., 2017). Biomass are normally rich in various types of metal elements (such
73 as K, Na, Ca, Mg and Fe) and can have different levels of N contents. Currently, there are
74 a series of knowledge gap on MCN formation during the production of biochar, for
75 example, (1) whether various inherent metals of biomass will exhibit synergistic or
76 antagonistic effects on MCN formation, (2) whether the anion of the biomass inherent
77 metal will affect the MCN formation, (3) whether the growth of MCN in a biochar can be
78 inhibited by the antagonistic effect of some metals. These questions need to be
79 addressed if we can continue to see biochar as an environmental asset.

80 Herein, and with the overall aim of developing a method to inhibit the formation of MCN
81 in biochar, we have first developed a prediction model for its formation on the basis of
82 original biomass characteristics. Secondly, MCN formation mechanisms in biochar are

83 systematically considered by both experimental and theoretical calculation methods.
84 Thirdly, some constraints on biochar production methods are adopted so as to inhibit MCN
85 formation. In this way, we can indeed achieve sustainable-biochar without the presence
86 of MCN.

87 **2. Materials and methods**

88 *2.1. Natural biomass and preparation of biochar*

89 18 types of biomass were collected from various industries of China and listed at
90 Supplementary Table S1 in details. These collected samples were freeze dried, then the
91 raw materials were crushed and sieved through a 40-mesh sieve. Biochar samples were
92 prepared *via* slow pyrolysis reaction under nitrogen gas (N₂) flow of 100 mL/min at 800 °C
93 (heating rate of 5 °C/min) for 1 h in a box-type resistance furnace (OFT-1200X, HF-Kejing
94 Co., Ltd., Anhui). The yield of the biochar samples was recorded, and the biochar samples
95 were stored in vacuum-sealed bags for further use. The mental elements of biomass are
96 detected by ICP-OES (5100/G8481A, Agilent, USA) after HNO₃-HClO₄-HF digestion.

97 To investigate the MCN formation mechanisms in biochar, plant protein (wheat protein)
98 with low ash content (< 1.0 %) was used as a basic N-containing biomass (12.4 %). While
99 K₂CO₃, Na₂CO₃, CaCO₃, MgC₂O₄, FeC₂O₄, KCl, K₂HPO₄, and K₂SO₄ were simulated as
100 inherent metal salts in biomass. The weight ratio of different metal salts and biomass was
101 1/10. Specially, the weight ratio of K₂CO₃ to biomass were further displayed at 0, 1/20,
102 1/10, and 1/5. The mixture of plant protein and inherent metal salt was shaken in aqueous

103 solution for 24 h, and then freeze-dried and heated up to 500 °C - 900 °C for 1 h under a
104 100 mL/min N₂ flow. The yield of the biochar samples was recorded, and the samples
105 were stored in vacuum-sealed bags for further use. Finally, to remove any inorganic salts,
106 the selected samples were thoroughly washed with HCl (2 M) and distilled water in a fume
107 hood, then dried in an oven at 100 °C overnight and filtered through a 100-mesh sieve.
108 For the inhibition study of MCN, MgCl₂ and FeCl₃ were acted as inhibitor with the weight
109 ratio to biomass is 0, 1/500, 1/50, 1/5.

110 *2.2. Characteristic of materials*

111 The CHNS analysis of the washed samples was performed using an elemental
112 analyzer (Vario EL III, Elementar, Germany). The crystal structures of samples (unwashed)
113 were determined by X'Pert PRO powder X-ray diffraction (XRD, Rigaku Ultimate IV, Japan)
114 equipped with Cu K α radiation between 2θ ranges of 10 – 80 °. The surface area and
115 porosity of the washed biochar were determined by nitrogen adsorption/desorption at -
116 196 °C using a Autosorb iQ2 instrument (Quantachrome, USA) after degassed at 300 °C
117 for 6 h. The surface area (S_{BET}) and total pore volume (V_{T}) were determined by the
118 Brunauer-Emmett-Teller (BET) equation. Pore size distribution was calculated with the
119 Density Function Theory (DFT) model.

120 The pyrolysis CO gas released in the sample's pyrolysis process was determined by
121 on-line mass spectrometry (MS, Hiden QIC-20, UK). Before MS analysis of CO, pyrolysis
122 oil was removed by tetrahydrofuran solution in solid CO₂ bath. The carrier gas and m/z

123 value for CO gas analysis was Ar and 28, respectively. CN⁻ content in solution was
124 quantitatively analyzed using an ion chromatograph (Dionex ICS-600, USA) with Abe
125 detector. The liquid solution was collected by the biochar samples soaked in NaOH
126 solution (0.1 mol/L) with ultrasonic dispersion for 30 mins at 25 °C. Specially, the CN⁻
127 content in samples with Ca, Mg, Fe are extracted based on the GB5085.3-2007. The
128 supernatant was then filtered using a 0.45 μm nylon membrane filter for further analysis.

129 *2.3. Absorption of bisphenol A*

130 To examine the changes of biochar adsorption ability, bisphenol A (BPA) is chosen as
131 target contaminant due to it is high frequently detected in surface water and its potential
132 toxicity to the environment. BPA adsorption isotherms were achieved in the concentration
133 of 2 - 100 mg/L with 50 mg/L biochar at 25 °C. After the adsorption equilibrium (16 h), the
134 supernatant was followed by filtration using a 0.45 μm polytetrafluoroethylene (PTFE)
135 membrane filter for analysis of BPA concentration. The concentration of BPA was
136 measured by UV/Vis spectrometer (TU-1901, Pgeneral, Beijing, China) at 280 nm
137 absorbance. *Langmuir* model was used to fit the adsorption isotherms.

138 *2.4. Characterization of bio-oil samples*

139 The molecular composition of bio-oil (collected in HPLC methanol) was analyzed by
140 the ESI FT-ICR MS (Bruker Apex ultra, Bruker, Germany) with a 9.4 T superconducting
141 magnet. The operating conditions for negative ion formation were conducted as our
142 previous study (Zhu et al., 2017). The mass range was set to m/z 200-800. In order to

143 enhance the signal-to-noise ratio and dynamic range, all of 128 scan FT-ICR data sets
144 were accumulated. Methodologies for FT-ICR MS mass calibration, data acquisition, and
145 processing have been described before (Liu et al., 2010). Scans of methanol were
146 performed as base-line to ensure that it was clean of the instrument before analyzing the
147 samples.

148 *2.5. Theoretical calculation details*

149 All calculations were carried out using Gaussian 6.0 program. Density functional theory
150 (DFT) computational method was used to optimize the equilibrium geometries of the
151 reactants, intermediates, transition states, and products. In the calculations, a geometry
152 optimization and frequency calculation are performed first at the B3LYP/6-31g* level and
153 then a subsequent frequency analysis is carried out at the B3LYP/def2svp level, also
154 obtained an overall energy barrier. Intrinsic reaction coordinate (IRC) calculations were
155 performed to ensure the correctness of each transition state.

156 **3. Results and discussion**

157 *3.1. MCN content in actual biomass derived biochar*

158 Many common types of biomass such as sawdust, wheat straw and livestock manure
159 show only small amounts of cyanide ion (CN⁻) in the resulting biochar. However, food
160 waste derived biochar (40286 mg/kg), phycocyanin derived biochar (85870 mg/kg) and
161 corn protein (with K₂CO₃) derived biochar (23251 mg/kg) have significant CN⁻ contents
162 (Supplementary Table S1). This can be correlated with the presence of abundant N and

163 K and Na content. Thus, CN^- content in biochar may significant effected by biomass
164 characteristics.

165 Fig. 1a displays the relationship between biomass characteristics and CN^- content in
166 the associated biochar using regression analysis to describe the possible conditions
167 associated with the production of MCN. The color bars represent the intensity of the R
168 value (multi-correlation coefficient), and a strong linear correlation is found between Na
169 content and CN^- content, indicating that Na is one dominating factor on MCN formation.
170 Na and CN^- content in 18 samples were further evaluated and it can be seen that the R^2
171 value is 0.63 after linear fitting (Fig. 1b). The red band is the 95 % confidence interval for
172 linear fitting (black solid line). It can be observed that, several dots are outside of the red
173 band (tag with a triangle). Some of the dots (No.1 and 2, are cow dung and biogas residue)
174 are associated with biomass samples which are rich in Na content but result in low CN^-
175 content. Both of these samples share a similar characteristic, which is abundance in Ca
176 and Fe in the biomass. This may imply that these two metals have a negative effect on
177 the formation of MCN during the biochar formation process. Another, a dot (No.3, corn
178 protein with K_2CO_3) corresponds to limited Na content but with high CN^- content; this is
179 because this sample contains a large amount of K. From these results it can be inferred
180 that, in comparison to Ca, Mg and Fe, the presence of alkali metals (such as K and Na)
181 in biomass may provide sites to support CN^- formation, an inference supported by the
182 Pearson correlation between the released CN^- and the metal content of biomass (Fig. 1c).

183 It should be pointed out that K content has not exhibited strong correlation with CN⁻
184 content in this diagram. This observation may be explained by the fact that abundant K-
185 containing samples are limited in studied samples, thus it couldn't observe obvious
186 positive tendency between K and CN⁻ content.

187 Lastly, the forecast model of CN⁻ content in biochar calculated and based on the
188 characteristics of biomass precursor is analyzed in a four-dimensional slice plot (Fig. 1d).
189 K content, Na content and the sum of Ca, Mg, Fe content in biomass are the independent
190 variables x , y and z , while the dependent variable (v) is the CN⁻ content in the biochar
191 (intensity of the color in the cube). The regression analysis equation is calculated as
192 following:

$$193 \quad v = 288.18 x + 1977.38 y - 341.22 z + 561.24 \quad (1)$$

194 This equation exhibits a good regression coefficient, $R^2=0.87$. It can be concluded that
195 the charring process of biomass can produce MCN in a process that is enhanced by alkali
196 metals (K and Na) but limited by Ca, Mg, and Fe. We must therefore be wary of biomass
197 with abundant alkali metal (such as food waste and marine) as raw material for biochar
198 production.

199 Additionally, with the background that biochar industry is in a rapidly development
200 supported by China government, more than 30% waste biomass in annual year will be
201 applied in biochar manufacturing (Wu et al., 2019). In these 18 types biomass samples,
202 corn straw (259 million tons per year, 2017) and fungi residue (92 million tons per year,

203 2017) are common biomass in China for biochar production. Based on above analysis,
204 their biochar can associate certain amount of MCN (105 mg/kg for corn straw derived
205 biochar and 251 mg/kg for fungi residue derived biochar, respectively). In such
206 circumstances, if 30 % (percentage of production in annual year in China) corn straw or
207 fungi residue is used to biochar production, considerable CN⁻ content can be generated
208 as a by-product, as shown in Supplementary Fig. S1. As can be clearly note that, these
209 generated CN⁻ content will increase the potential environment risk, especially in its
210 production process, environment application and soil carrier.

211 3.2. MCN production mechanism in biochar

212 As shown in Fig. 2a, the CN⁻ contents in biochar derived from biomass (plant protein)
213 with Na₂CO₃, K₂CO₃ and K₂SO₄ are 6972 mg/kg, 19116 mg/kg and 2555 mg/kg,
214 respectively. Typically, biomass with unstable O-containing alkali salts, such as alkali
215 carbonate (such as Na₂CO₃ or K₂CO₃) and alkali metal sulphates (such as K₂SO₄) exhibit
216 strong combination ability with organic nitrogen in biomass to yield MOCN and then to
217 MCN though carbothermal reduction (MOCN + C → MCN + CO). Results strongly suggest
218 that the metal salt present in the biomass plays an important role in MCN formation. It
219 seems that metals with higher valence (such as Ca, Mg and Fe) in biomass are less likely
220 to form MCN in the derived biochar, confirmed by the measured CN⁻ content in biochar
221 and the corresponding XRD pattern (Fig. 2a and Supplementary Fig. S2a). This failure is
222 believed due to the precursor MOCN not being formed in the biochar because organic N

223 is not well coordinated by such metals. These results agree well with the CN⁻ forecasting
224 model (Fig. 1d).

225 The formation curves of CO in peak 1 ($\text{KOCN} + \text{C} \rightarrow \text{KCN} + \text{CO}$) further confirms that
226 KCN can be produced in biochar derived from biomass containing K_2SO_4 and K_2CO_3
227 (Supplementary Fig. S2b and c). In contrast, K_2HPO_4 restricts KCN formation attributing
228 that ionized K^+ is firstly to complex with metaphosphate radical to form a stable substance
229 with cyclical structure (KPO_3), as indicated by corresponded XRD spectrum
230 (Supplementary Fig. S2b). KCl also blocks KCN formation since oxygen atoms are
231 needed for the formation of the critical intermediate KOCN. This mechanism will be further
232 analyzed by density functional theory method (DFT).

233 For depth study, K_2CO_3 is further used as specific inherent metal salt of biomass to
234 study the mechanism of MCN production. As show in Fig. 2a, the CN⁻ content in biochar
235 increases with pyrolysis temperature (from 500 to 800 °C), illustrating that the heating
236 temperature can facilitate the carbothermal reduction reaction. The distinct peak in the
237 XRD (especially $2\theta = 28^\circ$) of KCN in XRD also increases with increasing pyrolysis
238 temperature (Supplementary Fig. S3a) although it rapidly decreases after 900 °C due to
239 its volatilization (Fig. 2a). Increasing the K_2CO_3 content in biomass also increases the CN⁻
240 content in biochar (Fig. 2a), as suggested by the stronger intensity of KCN in the XRD
241 spectra (Fig. 2b). Thus, enhancement of the CO in peak 1 induced by KOCN reduction
242 ($\text{KOCN} + \text{C} \rightarrow \text{KCN} + \text{CO}$) further increased (Fig. 2c). In summary, MOCN from

243 complexation reaction between O-containing metal salt and organic N is the key precursor
244 to support MCN formation.

245 It also should be noted that this reaction consumes both carbon matrix and organic N,
246 thus simultaneously reducing the yield of biochar and its N content though boosting the
247 BET surface area of the biochar (after washing) (Fig. 2d and e). The strongly positive
248 correlation ($R^2=0.89$) between the yield of CO in peak 1 and the BET surface area of
249 biochar samples confirms that CO from carbothermal reduction reaction is the main pore-
250 foaming factor (Fig. 2e). Therefore, the changes in the biochar resulting from the
251 formation of MCN, including an improvement of micropore structure (Supplementary Fig.
252 3b), that can lead to the biochar having improved adsorption properties of organic
253 pollutant (Borchardt et al., 2017). Three samples with different BET surface areas were
254 selected for bisphenol A (BPA) absorption due to its potential toxicity to the environment
255 and highly detection frequency in surface water (Chen et al., 2016; Wang et al., 2016).
256 The samples are named A-x, where x indicates the different samples (Supplementary
257 Table S2). As can clearly be seen from Supplementary Fig. S3c, A-3 sample exhibits
258 excellent pollutant removal which can primarily be attributed to its improved porous
259 structure.

260 3.3. Mechanism of MCN formation calculated by DFT (density functional theory) method

261 As studied above, the requirement condition for KCN formation in biochar is the
262 complexation reaction between O-containing unstable K salt and organic N to form KOCN.

263 Therefore, DFT has been used to gain a deeper insight into the production mechanism of
264 KOCN. We first focused on the energy pathway for the decomposition of pyrrole to HCN,
265 pyrrole being a common N-containing pyrolysis species (Tian et al., 2014; Zhang et al.,
266 2014b). According to analysis of the bio-oil (Fig. 3a), compounds with DBE=5 and 6 are
267 associated to pyrrole-N or pyridine-N compounds. The intensity of these compounds in
268 the N₂ spectrum is significantly decreased for biomass containing K₂CO₃ (Fig. 3b). The
269 results imply that HCN can be released from the decomposition of pyrrole-N and pyridine-
270 N and the HCN can provide CN⁻ for KOCN formation (Chen et al., 2018). HCN is selected
271 as a typical example with CN⁻ containing compound from pyrolysis product of biomass for
272 K₂CO₃ complexation.

273 According to the calculation, after the internal hydrogen transfer and ring-opening of
274 pyrrole, one of the possible pathways of HCN formation is illustrated in detail in
275 Supplementary Fig. S4a, b. We then looked at the formation route of KOCN *via* reforming
276 of K₂CO₃ and HCN at high temperature. The energy barriers of the main reaction steps
277 are shown in Fig. 4a-c for two scenarios. In pathway one (Fig. 4a), CO₃²⁻ first complexes
278 with two HCN molecules to form a 7-membered heterocyclic compound, then in the
279 presence of K⁺, hydrogen migration reaction and dehydrogenation reaction occur.
280 Simultaneously, ring-opening of polycyclic compound is induced to further produce two
281 OCN's. Differing from pathway one, pathway two firstly involves complexation with HCN,
282 and an oxygen from CO₃²⁻ is reacted with HCN to form KOCN (Fig. 4b). With K⁺, the

283 hydrogen bond is broken to generate OCN^- . Another HCN is complexed to produce a new
284 compound (Fig. 4b, IM3). After that, reorganization of the structure produces a new OCN^- .
285 Comparison of the two paths for OCN^- production shows the energy barriers of transition
286 states in pathway one is much higher than in pathway two; meanwhile, from the reactants
287 to the products, the energy barriers are -44.92 kJ/mol and -169.55 kJ/mol, respectively,
288 indicating that pathway two is more favorable to OCN^- formation. The detail of energies
289 and relative energies of various compounds of respective states shows in Table S3 and
290 Table S4. We believe that the optimal pathway is mainly attributed to absence of ring
291 formation so that it proceeds *via* a very low energy transition state. Therefore, it can be
292 concluded that O-containing alkali salts play an important role in KOCN formation; it can
293 also be indirectly proven that biomass with KCl cannot complex with organic N to form
294 KOCN.

295 Additionally, the effects of Na^+ , Ca^{2+} and Mg^{2+} on OCN^- formation have been
296 determined in Fig. 4c, the energy barriers from IM1 to IM7 are -147.39 kJ/mol, 425.71
297 kJ/mol and 537.51 kJ/mol respectively. It was found that Ca^{2+} and Mg^{2+} lead to the higher
298 energy products, in contrast with K^+ and Na^+ in Fig. 4d. This may be attributed the hard
299 Lewis acidity of Na^+ and K^+ , which are good for open-loop reaction and hydrogen
300 migration (Li, 1993). Also, when the C-O is broken, they can stabilize products such as
301 OCN^- and H_2 (Khampuang et al., 2015). Thus, within this work, the theoretically proposed
302 pathways on OCN^- formation support the mechanism of MCN production. These

303 conclusions will play an important role in achieving a comprehensive understanding of
304 the OCN⁻ and further MCN formation during biomass charring.

305 *3.4. Inhibition mechanism of MCN during biomass pyrolysis*

306 MCN has been fully recognized to be a highly toxic substance (Manar et al., 2011; Choi
307 et al., 2012; Lee et al., 2015), thus, it urgently requires effective method to mitigate MCN
308 content in biochar. As above discussed, the inhibition of MCN can be achieved though
309 the blocking of MOCN formation, because MOCN is sole precursor of MCN. In addition,
310 it has been well documented that the oxygen atom from metal salts is important for
311 forming OCN⁻, and KCl cannot react with organic N to form KOCN. Therefore, if K₂CO₃
312 and metal chloride salt (e.g. MgCl₂, FeCl₃) in biomass can lead to a reaction to form a
313 thermally stable product such as KCl via metal recombination reaction, thus, KCN in
314 biochar can be completely inhibited due to lack of a precursor (KOCN) (Fig. 5a). As the
315 results show in Fig. 5b, MgCl₂ and FeCl₃ can well act as inhibitors to prevent the
316 production of MCN. When the addition of FeCl₃ is increased to 1/50 (the weight ratio
317 between FeCl₃ and biomass), CN⁻ content is reduced to 0 mg/kg. The XRD pattern of
318 biochar samples shows that, KCN is completely inhibited and only KCl and Fe₂O₃ can be
319 observed at this mass ration (insert Fig. 5b and Fig. 5c), a possible equation can be
320 considered as follow:



322 KCl and Fe₂O₃ are stable compounds and cannot easily form KOCN. Similar principles

323 can be applied to the reaction between K_2CO_3 and $MgCl_2$, when only KCl and MgO can
324 be detected in the XRD pattern (Fig. 5c).

325 Additionally, a successful application has been demonstrated in food waste (actual
326 waste biomass) derived biochar, and NaCN formation is completely inhibited after $FeCl_3$
327 treatment (Fig. 5d). It is also worth noting that NaCl and Fe_2O_3 can be observed in the
328 XRD pattern instead of NaCN (insert of Fig. 5d). Therefore, it is believed that high valence
329 metallic chlorides, such as $FeCl_3$ and $MgCl_2$, are efficient inhibitors to prevent MCN
330 production during biochar manufacturing, an extremely important conclusion for a rapidly
331 growing industry producing biochar (Zhu et al., 2016; Gou et al., 2019).

332 **4. Conclusions**

333 Alkali metals (such as Na and K) in biomass can induce the production of MCN in
334 biochar. However, Fe, Mg and Ca in biomass show antagonism with alkali metals during
335 pyrolysis and their presence inhibits MCN formation in biochar. Importantly, unstable O-
336 containing alkali salts in biomass (such as K_2CO_3 and Na_2CO_3) tend to complex with
337 organic N to produce MOCN. In turn, MOCN undergoes carbothermal reduction with the
338 carbon matrix and produces MCN. This process can promote the performance of biochar
339 but severely limits its application especially as an environmental remediator. To control
340 the formation of cyanide, we have proven a highly efficient and low-cost technology simply
341 involving metal chloride salts to completely inhibit CN^- formation in biochar. Thus, we can
342 envisage a way to deal with the potentially highly disrupting formation of toxic cyanide in

343 otherwise very useful biochar.

344 **Conflicts of interest**

345 There are no conflicts to declare.

346 **Acknowledgements**

347 This work was supported by the Shanghai Natural Science Foundation of China
348 (NO.19ZR1403800) and National Natural Science Foundation of China (No. 21876030).

349 **Appendix A. Supplementary data**

350 Supplementary data associated with this article can be found online at.

351 **References**

- 352 Borchardt, L., Zhu, Q.L., Casco, M.E., Berger, R., Zhuang, X., Kaskel, S., Feng, X., Xu, Q., 2017.
353 Toward a molecular design of porous carbon materials. *Mater. Today* 20, 592-610.
- 354 Chen, D., Kannan, K., Tan, H., Zheng, Z., Feng, Y.L., Wu, Y., Widelka, M., 2016. Bisphenol
355 analogues other than BPA: Environmental occurrence, human exposure, and toxicity—A
356 review. *Environ. Sci. Technol.* 50, 5438-5453.
- 357 Chen, H., Awasthi, S.K., Liu, T., Duan, Y., Ren, X., Zhang, Z., Pandey, A., Awasthi, M.K., 2020.
358 Effects of microbial culture and chicken manure biochar on compost maturity and
359 greenhouse gas emissions during chicken manure composting. *J. Hazard. Mater.* 389, 1-10.
- 360 Chen, W., Haiping, Y., Yingquan, C., Kaixu, L., Xia, M., Chen, H., 2018. Influence of biochar
361 addition on nitrogen transformation during copyrolysis of algae and lignocellulosic biomass.
362 *Environ. Sci. Technol.* 52, 9514-9521.
- 363 Choi, C.J., Berges, J.A., Young, E.B., 2012. Rapid effects of diverse toxic water pollutants on
364 chlorophyll a fluorescence: Variable responses among freshwater microalgae. *Water Res.*
365 46, 2615-2626.
- 366 Freddo, A., Cai, C., Reid, B.J., 2012. Environmental contextualisation of potential toxic elements
367 and polycyclic aromatic hydrocarbons in biochar. *Environ. Pollut.* 171, 18-24.
- 368 Ghidotti, M., Fabbri, D., Mašek, O., Mackay, C.L., Montalti, M., Hornung, A., 2017. Source and
369 biological response of biochar organic compounds released into water; relationships with
370 bio-oil composition and carbonization degree. *Environ. Sci. Technol.* 51, 6580-6589.
- 371 Gou, G., Meng, F., Wang, H., Jiang, M., Wei, W., Zhou, Z., 2019. Wheat straw-derived magnetic
372 carbon foams: In-situ preparation and tunable high-performance microwave absorption.
373 *Nano Research* 12, 1423-1429.
- 374 Hameed, R., Cheng, L., Yang, K., Fang, J., Lin, D., 2019. Endogenous release of metals with
375 dissolved organic carbon from biochar: Effects of pyrolysis temperature, particle size, and
376 solution chemistry. *Environ. Pollut.* 255, 1-10.
- 377 Hao, S., Zhu, X., Liu, Y., Qian, F., Fang, Z., Shi, Q., Zhang, S., Chen, J.M., Ren, Z., 2018.

378 Production temperature effects on the structure of hydrochar-derived dissolved organic
379 matter and associated toxicity. *Environ. Sci. Technol.* 52, 7486-7495.

380 Keiluweit, M., Kleber, M., Sparrow, M.A., Simoneit, B.R.T., Prah, F.G., 2012. Solvent-extractable
381 polycyclic aromatic hydrocarbons in biochar: Influence of pyrolysis temperature and
382 feedstock. *Environ. Sci. Technol.* 46, 9333-9341.

383 Khampuang, K., Boreriboon, N., Prasassarakich, P., 2015. Alkali catalyzed liquefaction of corncob
384 in supercritical ethanol–water. *Biomass Bioenergy* 83, 460-466.

385 Lee, J., Jang, J.H., Velusamy, N., Jung, H.S., Bhuniya, S., Kim, J., 2015. Intramolecular crossed-
386 benzoin reaction based KCN fluorescent probe in aqueous and biological environments.
387 *Chem. Commun.* 51, 7709-7712.

388 Li, C.J., 1993. Organic reactions in aqueous media - with a focus on carbon-carbon bond
389 formation. *Chem. Rev.* 93, 2023-2035.

390 Liao, S., Pan, B., Li, H., Zhang, D., Xing, B., 2014. Detecting free radicals in biochars and
391 determining their ability to inhibit the germination and growth of corn, wheat and rice
392 seedlings. *Environ. Sci. Technol.* 48, 8581-8587.

393 Lieke, T., Zhang, X., Steinberg, C.E.W., Pan, B., 2018. Overlooked risks of biochars: persistent
394 free radicals trigger neurotoxicity in *Caenorhabditis elegans*. *Environ. Sci. Technol.* 52, 7981-
395 7987.

396 Liu, P., Xu, C., Shi, Q., Pan, N., Zhang, Y., Zhao, S., Chung, K., 2010. Characterization of sulfide
397 compounds in petroleum: Selective oxidation followed by positive-ion electrospray fourier
398 transform ion cyclotron resonance mass spectrometry. *Anal. Chem.* 82, 6601-6606.

399 Lu, L., Guest, J.S., Peters, C.A., Zhu, X., Rau, G.H., Ren, Z.J., 2018. Wastewater treatment for
400 carbon capture and utilization. *Nat. Sustain.* 1, 750-758.

401 Luo, J., Jia, C., Shen, M., Zhang, S., Zhu, X., 2019. Enhancement of adsorption and energy
402 storage capacity of biomass-based N-doped porous carbon via cyclic carbothermal
403 reduction triggered by nitrogen dopant. *Carbon* 155, 403-409.

404 Manar, R., Bonnard, M., Rast, C., Veber, A.M., Vasseur, P., 2011. Ecotoxicity of cyanide

405 complexes in industrially contaminated soils. *J. Hazard. Mater.* 197, 369-377.

406 Oleszczuk, P., Joško, I., Kuśmierz, M., 2013. Biochar properties regarding to contaminants
407 content and ecotoxicological assessment. *J. Hazard. Mater.* 260, 375-382.

408 Opatokun, S.A., Strezov, V., Kan, T., 2015. Product based evaluation of pyrolysis of food waste
409 and its digestate. *Energy* 92, 349-354.

410 Qiu, M., Sun, K., Jin, J., Han, L., Sun, H., Zhao, Y., Xia, X., Wu, F., Xing, B., 2015. Metal/metalloid
411 elements and polycyclic aromatic hydrocarbon in various biochars: The effect of feedstock,
412 temperature, minerals, and properties. *Environ. Pollut.* 206, 298-305.

413 Quan, G., Fan, Q., Sun, J., Cui, L., Wang, H., Gao, B., Yan, J., 2020. Characteristics of organo-
414 mineral complexes in contaminated soils with long-term biochar application. *J. Hazard.*
415 *Mater.* 384, 1-12.

416 Sevilla, M., Ferrero, G.A., Diez, N., Fuertes, A.B., 2018. One-step synthesis of ultra-high surface
417 area nanoporous carbons and their application for electrochemical energy storage. *Carbon*
418 131, 193-200.

419 Sigmund, G., Huber, D., Bucheli, T.D., Baumann, M., Borth, N., Guebitz, G.M., Hofmann, T., 2017.
420 Cytotoxicity of biochar: A workplace safety concern? *Environ. Sci. Technol. Lett.* 4, 362-366.

421 Smith, C.R., Hatcher, P.G., Kumar, S., Lee, J.W., 2016. Investigation into the sources of biochar
422 water-soluble organic compounds and their potential toxicity on aquatic microorganisms.
423 *Acs Sustain. Chem. Eng.* 4, 2550-2558.

424 Stefaniuk, M., Oleszczuk, P., Bartmiński, P., 2016. Chemical and ecotoxicological evaluation of
425 biochar produced from residues of biogas production. *J. Hazard. Mater.* 318, 417-424.

426 Sun, K., Kang, M., Zhang, Z., Jin, J., Wang, Z., Pan, Z., Dongyu, X., Wu, F., Xing, B., 2013. Impact
427 of deashing treatment on biochar structural properties and potential sorption mechanisms
428 of phenanthrene. *Environ. Sci. Technol.* 47, 1473-11481.

429 Tian, K., Liu, W.J., Qian, T., Jiang, H., Yu, H.Q., 2014. Investigation on the evolution of N-
430 containing organic compounds during pyrolysis of sewage sludge. *Environ. Sci. Technol.* 48,
431 10888-10896.

432 Tsubouchi, N., Nishio, M., Mochizuki, Y., 2016. Role of nitrogen in pore development in activated
433 carbon prepared by potassium carbonate activation of lignin. *Appl. Surf. Sci.* 371, 301-306.

434 Wang, P., Xiao, P., Zhong, S., Chen, J., Lin, H., Wu, X.L., 2016. Bamboo-like carbon nanotubes
435 derived from colloidal polymer nanoplates for efficient removal of bisphenol A. *J. Mater.*
436 *Chem. A* 4, 15450-15456.

437 Wang, T., Sun, H., Ren, X., Li, B., Mao, H., 2017. Evaluation of biochars from different stock
438 materials as carriers of bacterial strain for remediation of heavy metal-contaminated soil. *Sci.*
439 *Rep.* 7, 1-10.

440 Wu, P., AtaUlKarim, S.T., Singh, B.P., Wang, H., Wu, T., Liu, C., Fang, G., Zhou, D., Wang, Y.,
441 Chen, W., 2019. A scientometric review of biochar research in the past 20 years (1998–
442 2018). *Biochar* 1, 23-43.

443 Yue, Y., Shen, C., Ge, Y., 2019. Biochar accelerates the removal of tetracyclines and their
444 intermediates by altering soil properties. *J. Hazard. Mater.* 380, 1-12.

445 Zhang, G., Ma, D., Peng, C., Liu, X., Xu, G., 2014a. Process characteristics of hydrothermal
446 treatment of antibiotic residue for solid biofuel. *Chem. Eng. J.* 252, 230-238.

447 Zhang, J., Lü, F., Zhang, H., Shao, L., Chen, D., He, P., 2015. Multiscale visualization of the
448 structural and characteristic changes of sewage sludge biochar oriented towards potential
449 agronomic and environmental implication. *Sci. Rep.* 5, 1-8.

450 Zhang, J., Tian, Y., Zhu, J., Zuo, W., Yin, L., 2014b. Characterization of nitrogen transformation
451 during microwave-induced pyrolysis of sewage sludge. *J. Anal. Appl. Pyrolysis* 105, 335-
452 341.

453 Zhang, Y., Yang, R., Si, X., Duan, X., Quan, X., 2019. The adverse effect of biochar to aquatic
454 algae- the role of free radicals. *Environ. Pollut.* 248, 429-437.

455 Zhao, L., Zhao, Y., Nan, H., Yang, F., Qiu, H., Xu, X., Cao, X., 2020. Suppressed formation of
456 polycyclic aromatic hydrocarbons (PAHs) during pyrolytic production of Fe-enriched
457 composite biochar. *J. Hazard. Mater.* 382, 1-9.

458 Zhu, X., Liu, Y., Qian, F., Lei, Z., Zhang, Z., Zhang, S., Chen, J., Ren, Z.J., 2017. Demethanation

459 trend of hydrochar induced by organic solvent washing and its influence on hydrochar
460 activation. *Environ. Sci. Technol.* 51, 10756-10764.

461 Zhu, X., Qian, F., Liu, Y., Matera, D., Wu, G., Zhang, S., Chen, J., 2016. Controllable synthesis of
462 magnetic carbon composites with high porosity and strong acid resistance from hydrochar
463 for efficient removal of organic pollutants: An overlooked influence. *Carbon* 99, 338-347.

464

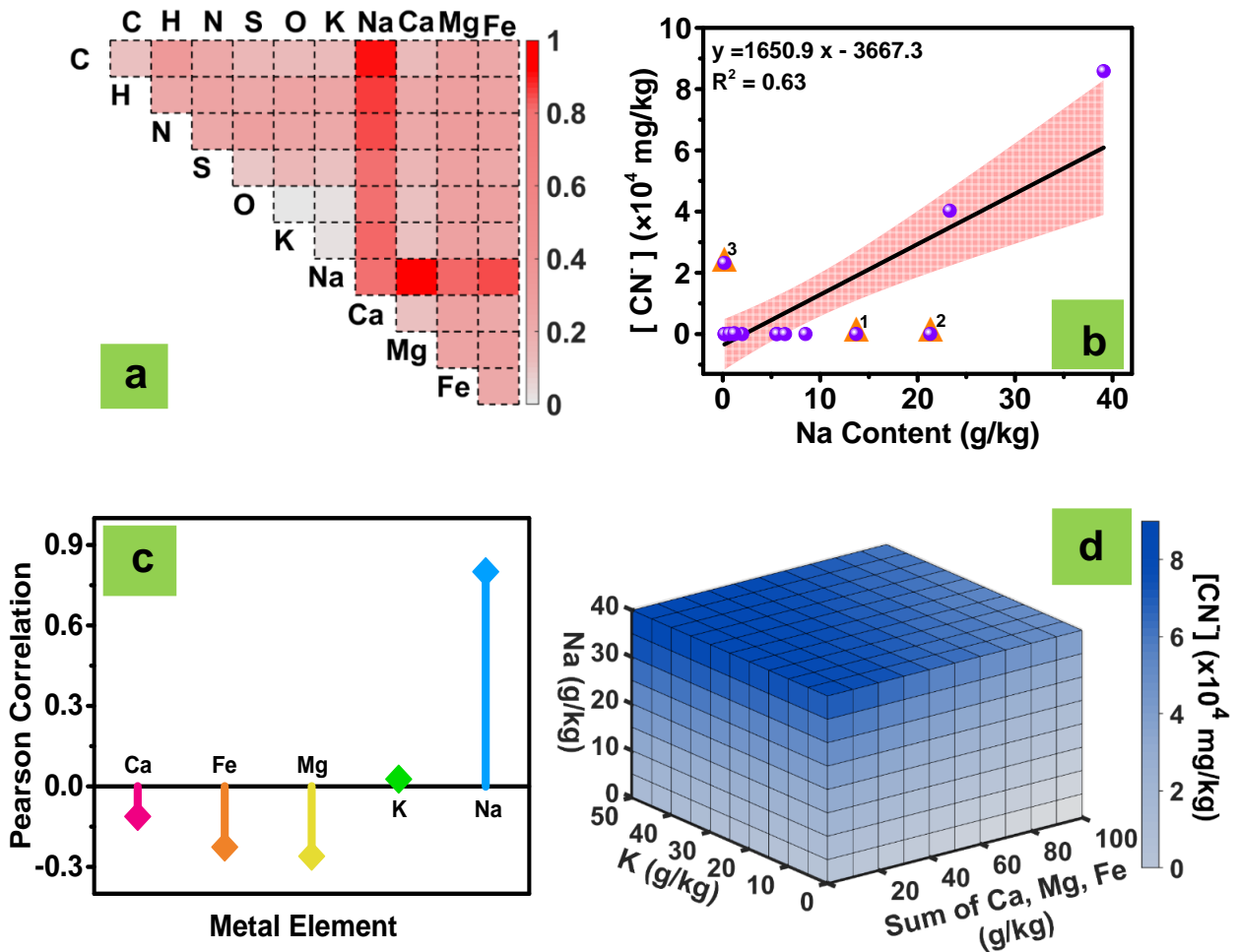


Fig. 1 (a) Regression analysis between the released CN⁻ content and characteristics of raw materials, the color bars represent the intensity of R value (multi-correlation coefficient); (b) correlations of Na content in raw materials and released CN⁻ content in biochar; (c) Pearson correlation of CN⁻ content in biochar and metal elements in raw materials; (d) 4D slice plot of released CN⁻ content in biochar and Na content, K content and the sum of Ca, Mg, Fe content in raw materials.

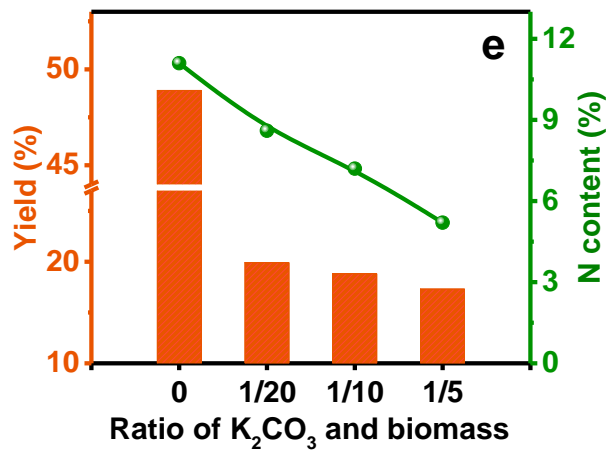
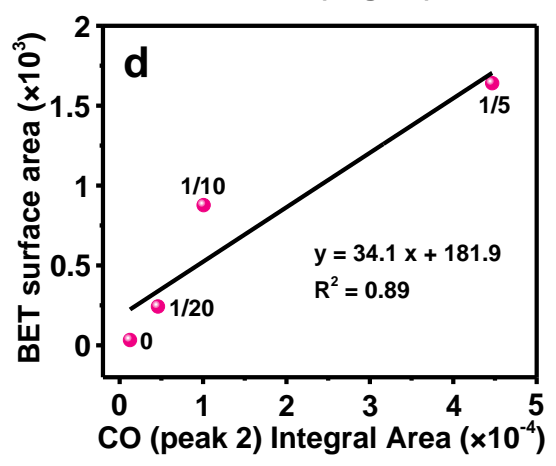
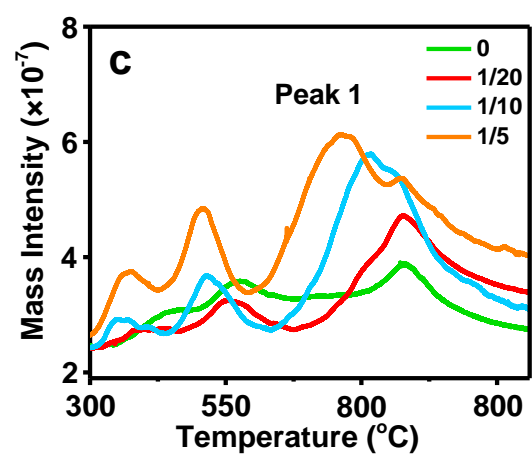
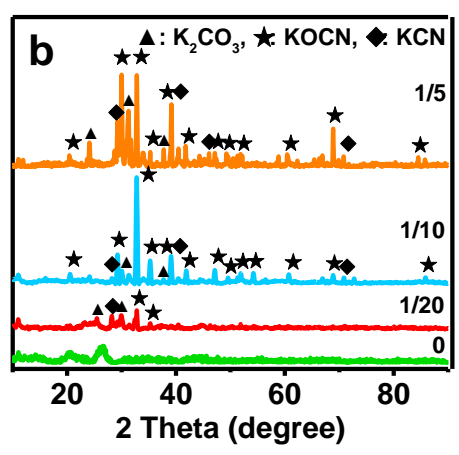
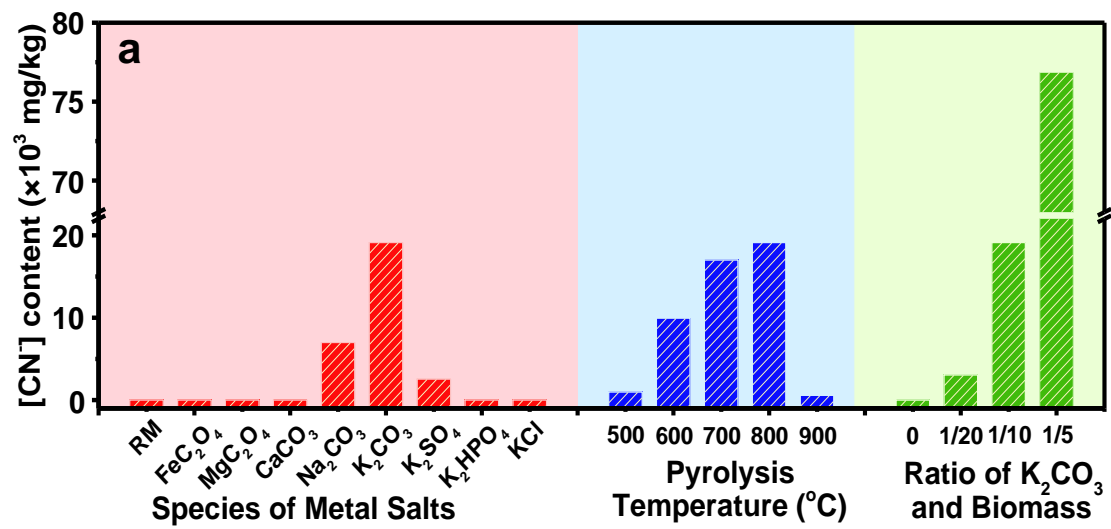


Fig. 2 (a) The CN⁻ content in biochar under different pyrolysis conditions (RM: raw material, Species of salt metals: pyrolyzed at 800 °C, the ratio of metal salt and biomass is 1/10; Pyrolysis temperature: 500 °C - 900 °C, the ratio of inorganic metal salt and biomass is 1/10; Ratio of K₂CO₃ and biomass: pyrolyzed at 800 °C.); (b) XRD patterns of unwashed samples pyrolyzed at various ratio of K₂CO₃ and biomass; (c) CO release curves from biochar pyrolyzed at various ratio of K₂CO₃ and biomass; (d) correlation between CO integral area in peak 1 and BET surface area for biochar (after washed samples) from pyrolyzed at different ratio of K₂CO₃ and biomass; (e) the yield and N content of washed biochar pyrolyzed at various ratio of K₂CO₃ and biomass.

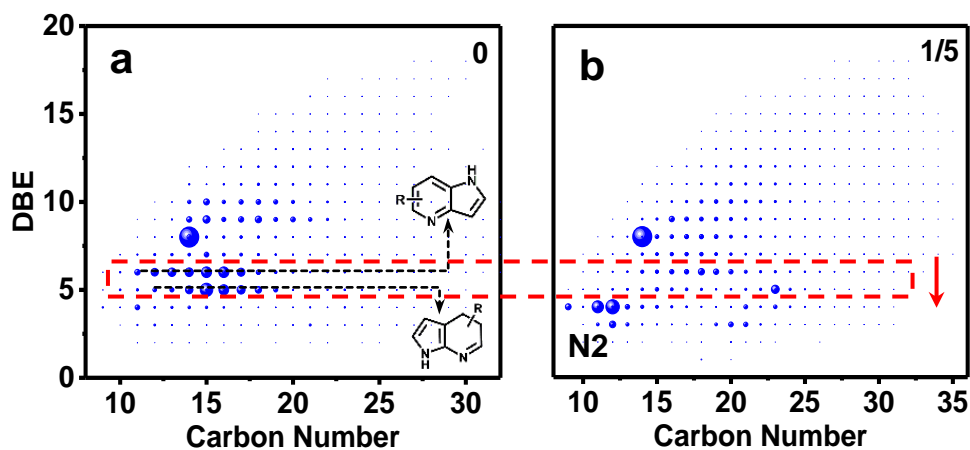


Fig. 3 (a) DBE versus carbon number for the N2 class species in bio-oil (collected from pyrolysis and the weight ratio of K_2CO_3 and biomass is 0); (b) DBE versus carbon number for the N2 class species in bio-oil (collected from pyrolysis and the weight ratio of K_2CO_3 and biomass is 1/5).

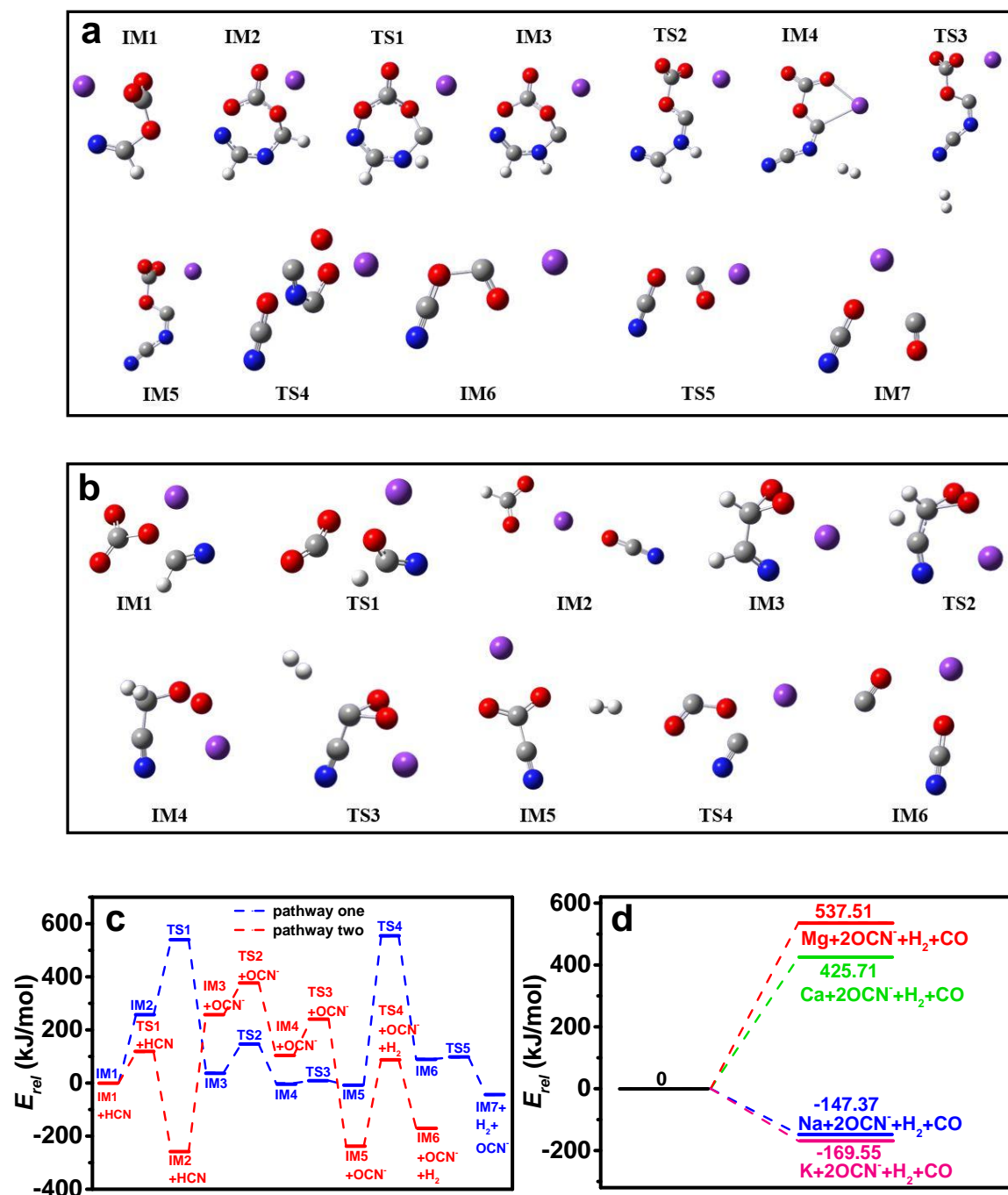


Fig. 4 (a) and (b) Optimized geometries of the reactants intermediates (IM), transition states (TS) and products in the reaction between HCN, CO_3^{2-} and K^+ at B3LYP/def2svp. The blue spheres represent nitrogen atoms; the red spheres represent oxygen atoms;

the grey spheres represent carbon atoms; the white spheres represent hydrogen atoms; the violet spheres represent potassium atoms; (c) Potential energy surface of the reaction HCN, CO_3^{2-} and K^+ calculated at B3LYP/def2svp; (d) Potential energy surface of the reaction HCN, CO_3^{2-} , and different metal ions calculated at B3LYP/def2svp.

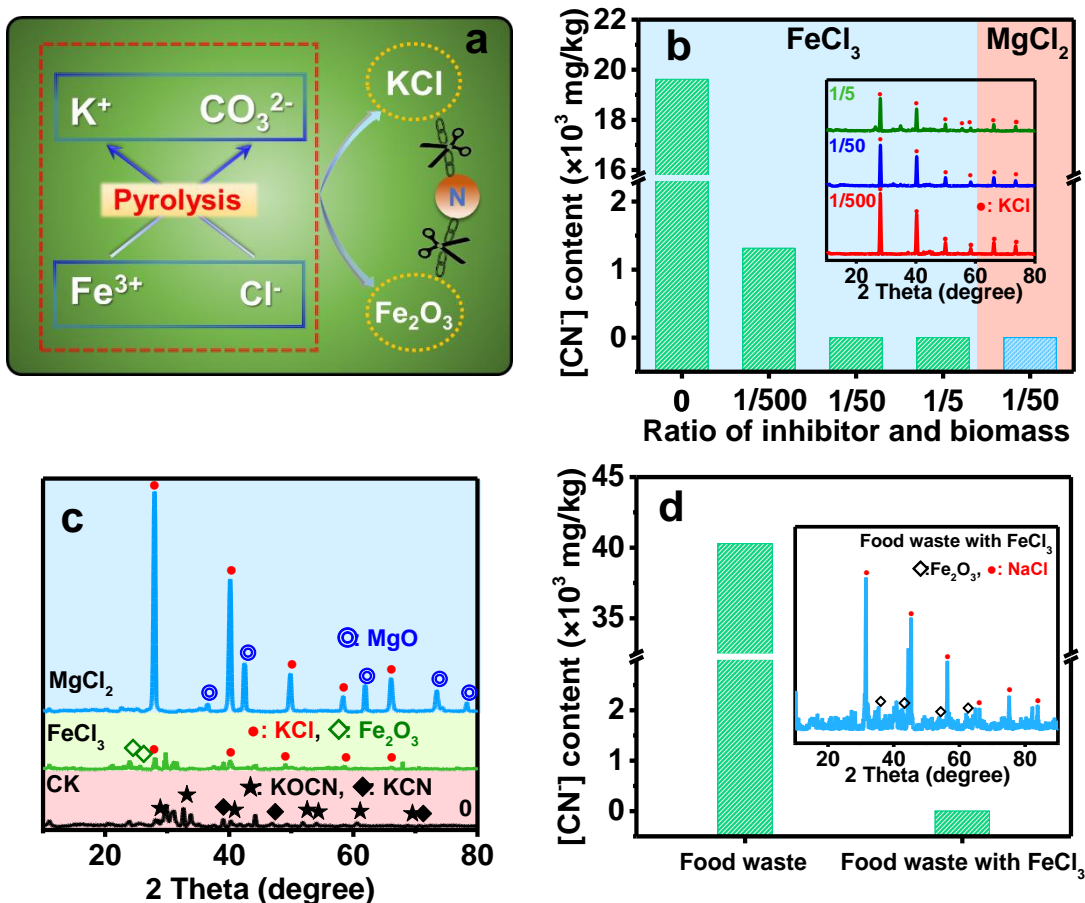


Fig. 5 (a) Interaction between K_2CO_3 and $FeCl_3$ for MCN inhibition; (b) The CN^- content in biochar after pyrolyzed with various ratio of $FeCl_3/MgCl_2$ and biomass (with K_2CO_3); insert: XRD pattern of unwashed samples pyrolyzed from various weight ratio of $FeCl_3$ and biomass; (c) XRD patterns of the samples from pyrolyzed with various metal chloride and biomass (CK: wheat protein with K_2CO_3 , the weight ratio between K_2CO_3 and biomass is 1/10; $FeCl_3$ treatment: the weight ratio between $FeCl_3$ and CK is 1/50, after washed sample; $MgCl_2$ treatment: the weight ratio between $MgCl_2$ and CK is 1/50, unwashed sample); (d) The CN^- content in food waste-derived biochar with and without $FeCl_3$ treatment (the weight ratio between $FeCl_3$ and food waste is 1/50); insert: XRD pattern of food waste-derived biochar pyrolyzed with $FeCl_3$.